Droplet Spreading: Partial Wetting Regime Revisited

M. J. de Ruijter,[†] J. De Coninck,*[,†] and G. Oshanin[†,‡]

Centre de Recherche en Modélisation Moléculaire, Université de Mons-Hainaut, 20 Place du Parc, 7000 Mons, Belgium, and Laboratoire de Physique Théorique des Liquides, Université Pierre et Marie Curie, T.16, 4 place Jussieu, 75252 Paris Cedex 05, France

Received December 1, 1997. In Final Form: August 21, 1998

We study the time evolution of a sessile liquid droplet, which is initially put onto a solid surface in a nonequilibrium configuration and then evolves towards its equilibrium shape. We adapt here the standard approach to the dynamics of mechanical dissipative systems, in which the driving force, i.e., the gradient of the system's Lagrangian function, is balanced against the rate of the dissipation function. In our case, the driving force is the loss of the droplet's free energy due to the increase of its base radius, whereas the dissipation occurs because of viscous flows in the core of the droplet and frictional processes in the vicinity of the advancing contact line, associated with attachment of fluid particles to solid. Within this approach, we derive closed-form equations for the evolution of the droplet's base radius and specify regimes at which different dissipation channels dominate. Our analytical predictions compare very well with experimental data.

I. Introduction

Many industrial and material processing operations require the spreading of a liquid on a solid. To name but a few, we might mention coating and painting, plant protection, glueing, oil recovery from porous rocks, and lubrication. Consequently, the liquid may be a paint, a lubricant, an ink, or a dye. The solid may either have a simple surface or be finely divided, as in the case of suspensions, porous media, or fibers.[1−8]

Apart from the fundamental problem of whether a given solid is wetted by the liquid in question, many of the practical applications require precise knowledge of the rates of the wetting processes. Particularly, one is often interested to know how fast a liquid droplet, when deposited on a solid substrate, can wet a given area of the solid surface.

In this regard, two different types of descriptions of sessile droplet spreading exist: hydrodynamic and molecular kinetic, which differ from each other mostly in the consideration of the dominant dissipation channel.[1,3−8] The first approach emphasizes the dissipation due to viscous flows generated in the core of the spreading droplet. Within this approach, which has been scrutinized by many authors during the last several decades,[9−16] a relation between the capillary number Ca and the value of the contact angle $\theta(t)$ has been derived. This relation, which represents a zeroth-order approximation in the expansion in powers of the capillary number, yields simple scaling laws determining the time evolution of the contact angle and the droplet's base radius $R(t)$. In case of spreading circular droplets, one finds $R(t) \sim t^{1/10}$ and $\theta(t) \sim t^{-3/10}$. These scaling laws have been examined experimentally and shown to agree fairly well with experimental data for many liquid/solid systems.[8−12,16,17] On the other hand, early studies by Sawicki,[17] who has examined experimentally spreading rates of liquid droplets composed of PDMS polymers having different molecular weights (and different viscosities), have demonstrated pronounced departures from the $R(t) \sim t^{1/10}$ behavior for liquids of progressively lower viscosity. Moreover, it has been realized (for example, see Cazabat et al.[4] for a general discussion) that fitting experimental data to hydrodynamic descriptions (which presume certain cut-off is at short length scales or small contact angles) often leads to unreasonably small values of these empirical cut-off parameters, which fall below molecular size.

The second approach, which originates from the molecular kinetic theory of Eyring,[19] has been adapted to describe the kinetics of wetting phenomena by Blake[18] Blake and Hayes,[18] and Cherry and Holmes[20] and was subsequently developed by others.[6,21,22] In contrast to the hydrodynamic picture, this approach concentrates on the dissipative processes occurring in the vicinity of the advancing contact line, which stem from the attachment of fluid particles to a solid, and ignores the dissipation due to viscous flows in the core of the liquid droplet. In

[†] Université de Mons-Hainaut.

[‡] Université Pierre et Marie Curie.

(1) de Gennes, P. G. *Rev. Mod. Phys.* **1985**, *57*, 827. de Gennes, P. G. In *Liquids at Interfaces*; Chavrolin, J., Joanny, J. F., Zinn-Justin, J., Eds.; North-Holland: New York, 1990; p 371.

(2) Brochard-Wyart, F.; de Gennes, P. G. *Adv. Colloid Interface Sci.* **1992**, *39*, 1.

(3) Cazabat, A. M. *Contemp. Phys.* **1987**, *28*, 347.

(4) Cazabat, A. M.; Gerdes, S.; Valignat, M. P.; Villette, S. *Dynamics of Wetting: From Theory to Experiment, Surface Science*, in press.

(5) Dussan, E. B., V. *Ann. Rev. Fluid Mech.* **1979**, *11*, 371.

(6) Blake, T. D. In *Wettability*; Berg, J. C., Ed.; Marcel Dekker: New York, 1993.

(7) De Coninck, J. *Colloids Surf.* **1996**, *114*, 155.

(8) Marmur, A. *Adv. Colloid Interface Sci.* **1983**, *19*, 75.

(9) Ogarev, V. A.; Timonina, T. N.; Arslanov, V. V.; Trapeznikov, A. A. *J. Adhes.* **1974**, *6*, 337.

(10) Voinov, O. V. *Fluid Dynamics* **1976**, *11*, 714.

(11) Tanner, L. H. *J. Phys.* **1979**, *D2*, 1473.

(12) Hoffmann, R. *J. Colloid Interface Sci.* **1975**, *50*, 228.

(13) Cox, R. G. *J. Fluid. Mech.* **1986**, *168*, 169.

(14) de Gennes, P. G.; Hua, X.; Levinson, P. *J. Fluid. Mech.* **1990**, *212*, 55.

(15) Seaver, A. S.; Berg, J. C. *J. Appl. Polym. Sci.* **1994**, *52*, 431.

(16) Cazabat, A. M.; Cohen-Stuart, M. *J. Phys. Chem.* **1986**, *90*, 5845.

(17) Sawicki, G. In *Wetting, Spreading and Adhesion*; Padday, J. F., Ed.; Academic: New York, 1978.

(18) Blake, T. D. The Contact Angle and Two-Phase Flow. Ph.D. Thesis, University of Bristol, 1968. Blake, T. D.; Haynes, J. M. *J. Colloid Interface Sci.* **1969**, *30*, 421.

(19) Glasstone, S.; Laidler, K. J.; Eyring, H. J. *The Theory of Rate Processes*; McGraw-Hill: New York, 1941.

(20) Cherry, B. W.; Holmes, C. M. *J. Colloid Interface Sci.* **1969**, *29*, 174.

(21) Dodge, F. T. *J. Colloid Interface Sci.* **1988**, *121*, 155.

(22) Ruckenstein, E.; Dunn, M. *J. Colloid Interface Sci.* **1976**, *56*, 460; *59*, 137.

10.1021/la971301y CCC: $18.00
Published on Web 02/26/1999

this approach, one finds for the dynamics of the base radius and contact angle $R(t) \sim t^{1/7}$ and $\theta(t) \sim t^{-3/7}$, respectively. These laws have also been shown to work fairly well for some experimental liquid/solid systems,[8,21] which apparently contradicts the behavior reported by others.[8−12,16,17] The origin of this discrepancy was under debate for a long time.

On the other hand, it has been clearly understood that both types of dissipation do exist simultaneously, and several attempts to work out a combined theory have been made. In particular, a simple way of formulating a combined theory on the basis of the molecular kinetic approach was discussed by Blake.[6] It was supposed here that the effects of viscous flows can be incorporated into the molecular kinetic approach directly, by simple adding to the barriers created by the liquid/solid attractions a viscous contribution. This procedure results, however, in equations which have essentially the same structure as those originally found by others[18] (apart from some renormalization of coefficients, which now include the liquid's viscosity) and thus can not reproduce the experimentally seen $R(t) \sim t^{1/10}$ behavior. Another way of thought has been put forward in the paper by Voinov,[10] who has conjectured an equation relating the value of the microscopic cut-off angle θ_c, which is artificially introduced in macroscopic hydrodynamic descriptions in order to remove essential singularities and nonhydrodynamic dissipation (hereafter denoted as $T\sum_l$). This idea has been subsequently developed by Petrov and Petrov,[23] who have combined heuristically the relation between the contact angle $\theta(t)$ and the capillary number Ca, obtained in terms of essentially *macroscopic* hydrodynamic theory, the Voinov's relation between the *microscopic* angle θ_c and $T\sum_l$, and the Blake and Haynes expression for the contact line velocity, which holds, in terms of this approximate approach, for any value of Ca. Combination of these three relations allowed for the derivation of a closed-form expression for the contact line velocity as the function of the parameters of the liquid/solid system in question. Evidently, the resulting expression can serve as a very useful interpolation formula, but care should be exercised in interpreting the fitting parameters as physical quantities because this effective approach is clearly empirical. Lastly, a rather different approach has been put forward by de Gennes in his analysis of the energy dissipation in the precursor film.[1] It was suggested in this work that the unbalanced capillary force should be compensated by the total energy dissipation occurring during the spreading process: namely, the viscous dissipation in the core of the droplet, the dissipation at the advancing contact line, and that in a precursor film. In this analysis, however, the emphasis was put in the latter dissipation channel, and the energy dissipation due to frictional processes in the vicinity of the liquid/solid interface was intentionally neglected. On the basis of this analysis, it has been claimed afterwards by Brochard-Wyart and de Gennes[2] that it is most likely that nonhydrodynamic dissipation dominates at relatively large values of the contact angle and the hydrodynamic dissipation channel prevails at smaller angles. However, no selection of the kinetic regimes associated with different dissipation channels has been performed within this physically meaningful approach.

In the present paper, we develop a macroscopic dynamic description of a sessile liquid droplet spreading on solid surface in a situation appropriate for partial wetting, i.e., such that the macroscopic spreading power characterizing the liquid/solid system in question is negative. In our approach, we take into account two different dissipation channels: dissipation due to viscous flows and that due to frictional processes in the vicinity of the contact line. Dissipation in the precursor film, which is not a generic feature for partial wetting, is not considered here. To describe the time evolution of the droplet, we adapt the standard mechanical approach to dissipative system dynamics,[24] in which the driving force, the gradient of the system's Lagrangian function, is balanced by the rate of total dissipation. In our case, the driving force is the loss of the droplet's free energy due to the increase in the base radius. Consequently, our approach complements that proposed by de Gennes.[1] Furthermore, we derive closed-form equations describing the time evolution of the droplet's base radius and discuss several possible kinetic regimes associated with different dissipation channels. We show that, as it was expected intuitively, both dissipation channels may be important, but they have a dominant effect on the kinetics of the wetting process at different time scales: namely, nonhydrodynamic dissipation resulting in the law $R(t) \sim t^{1/7}$ prevails at relatively short times, and hydrodynamic dissipation which yields the $t^{1/10}$ law represents the dominant dissipation channel at long times. Moreover, we find explicitly the crossover time separating these two regimes; we show that it may be very large for liquids with low viscosity or substrates with high friction coefficients, such that the $t^{1/10}$ law will show up only at very long times, which is in agreement with the trend observed by Sawicki.[17,21] This allows us to conclude that those experiments which show the departure from the $R(t) \sim t^{1/10}$ behavior are apparently performed with liquid/solid systems with the crossover time sufficiently large compared to the time scale of observation. On the other hand, experiments which reveal such a law are done with systems with low values of the crossover time.

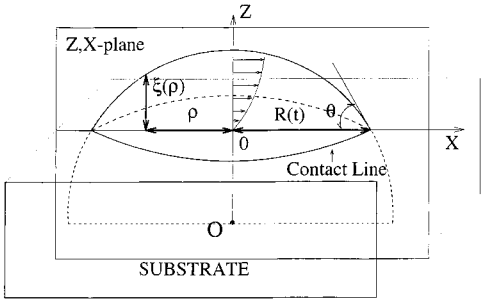

Figure 1. Schematic picture of a sessile droplet spreading on a solid substrate.

Our paper is structured as follows. In Section 2, we formulate our model and present the basic equations. In Section 3, we propose a comparison between the general analytical equations, derived in Section 2, and experimental data. Section 4 is devoted to the analysis of different asymptotical regimes, which stem from the different dissipation channels. Finally, in Section 5, we conclude with a brief discussion of our results.

II. The Model and Basic Equations

Consider a nonvolatile, sessile liquid droplet of volume V, which is placed at time $t = 0$ on an ideal horizontal solid substrate, and exposed to a neutral gas phase, for example, air. We suppose that the initial shape of the droplet is part of a sphere, which is characterized by the base radius R_0 and the macroscopic contact angle θ_0 (see Figure 1).

(23) Petrov, P. G.; Petrov, J. G. *Langmuir* **1992**, *8*, 1762.

(24) Landau, L. D.; Lifschitz, E. M. *Mechanique*, 3rd ed.; Edition MIR: Moscou, 1969.

For simplicity, we will suppose in what follows that $\theta_0 \leq {}^{\pi}/_{2}$.

The key parameter, which defines the qualitative behavior of the liquid droplet on a given substrate, is the spreading power S. Explicitly, S is given by

$$S = \gamma_{SG} - \gamma - \gamma_{SL} \tag{1}$$

where γ_{SG}, γ, and γ_{SL} denote the solid/gas, liquid/gas and solid/liquid interfacial tensions, respectively.

When $S \geq 0$, the droplet spreads spontaneously and tends to shield the solid from the gas phase. In the conventional macroscopic picture, the droplet spreads completely such that the final stage is a liquid layer, covering the solid surface. More elaborate theoretical descriptions have demonstrated, however, that this is not necessarily so and spreading may cease when the height at the apex of the droplet falls to mesoscopic or microscopic scales (for example, see de Gennes[1]). At such scales the disjoining pressure, which tends to thicken the droplet, becomes essential and competes effectively against the capillary forces; in consequence, an equilibrium pancake-like structure may arise instead of the molecular film. The thickness of this extended structure is determined by the interplay between the spreading power and the liquid/gas interfacial tension γ.

When $S < 0$, the liquid droplet partially wets the solid. Depending on its initial shape, the macroscopic droplet may contract or dilate, but it eventually reaches an equilibrium spherical caplike shape. In the present work, we will be concerned only with the latter case, supposing that the spreading power is negative. Consequently, in the situation under study, a liquid droplet, which is characterized initially by the base radius R_0 and the contact angle θ_0, will spread on the solid substrate until it reaches an equilibrium shape with base radius R_{eq} and contact angle θ_{eq} ($\theta_{eq} > 0$), which obeys the Young's equation, written here as

$$cos\ \theta_{eq} = 1 + \frac{S}{\gamma} \tag{2}$$

Further on, we will suppose that the droplet, which is placed initially in a nonequilibrium configuration, retains the ideal spherical cap form at any moment in time. This implies that the instantaneous configuration of the droplet can be totally described by a single parameter: it is either the time-dependent base radius $R(t)$, the contact angle $\theta(t)$, or the height at the apex of the droplet $h(t)$. Measuring, for instance, the instantaneous base radius, we can calculate the corresponding values of the dynamic contact angle by virtue of the conservation of volume condition, which gives

$$\frac{R^3(t)}{V} = \frac{3}{\pi}\phi[\theta(t)] \tag{3}$$

where

$$\phi[\theta(t)] = \frac{[1 + \cos\theta(t)]\sin\theta(t)}{[1 - \cos\theta(t)][2 + \cos\theta(t)]} \tag{4}$$

The corresponding height at the apex of the droplet is then determined by

$$h(t) = R(t)\frac{[1 - \cos\theta(t)]}{\sin\theta(t)} \tag{5}$$

We hasten to remark, that such an approximation is used here only for the derivation of simple explicit formulae. Any other relationship between the contact angle and the base radius could be incorporated within our approach but would not significantly change the results. Moreover, our approximation is appropriate in its own right when several reasonable physical conditions are fulfilled.[25−28] First, the droplet has to be sufficiently small, such that the bond number is small and thus gravity effects can be ignored. Second, attractive liquid/solid interactions (say, van der Waals interactions) are to be sufficiently short-ranged. As a matter of fact, the interactions with the substrate will always distort the liquid edge in the vicinity of the substrate. We suppose here that the typical size of the distorted region, which is normally microscopically or mesosocopically large, is much smaller than the characteristic scale of observation. Lastly, the viscosity of the liquid droplet has to be not very large. It is known, for instance, that for high-viscosity liquids, such as liquids composed of polymers with high molecular weight, only the upper part of the droplet can be well-approximated by a spherical cap; closer to the substrate there appears a microscopically large protruded region, the so-called "foot."

Within the spherical cap approximation, the potential energy of the gas/liquid/solid system can be written as a function of $R(t)$ only. The associated free energy is then given by

$$F\{R(t)\} = \pi R^2(t)(\gamma_{SL} - \gamma_{SG}) + 2\pi\gamma\int_0^{R(t)} \rho\, d\rho\sqrt{1 + [d\xi(\rho)/d\rho]^2} \tag{6}$$

where the terms under the integral describe, in the usual fashion, the surface energy of the droplet, and the other terms give the contributions due to the tensions of the solid/gas and solid/liquid interfaces. The function $\xi(\rho)$ defines the height of the droplet at distance ρ from the symmetry axis (see Figure 1). From eqs 3 and 4, we find that for fixed $R(t)$ the local height $\xi(\rho)$ obeys

$$\xi(\rho) = \frac{R(t)}{\sin\theta(t)}\left[\left(1 - \frac{\rho^2\sin^2\theta(t)}{R^2(t)}\right)^{1/2} - \cos\theta(t)\right] \tag{7}$$

Let us now consider the spreading dynamics and address the question of how a droplet with initial radius R_0 evolves in time to the equilibrium state with base radius R_{eq}. To do this, we consider the droplet as a purely mechanical system, the configuration of which is uniquely defined by eq 5 [in fact, by the instantaneous value of $R(t)$], and relate it to the total dissipation occurring during the change in the droplet radius from the value $R(t)$ to the value $R(t) + \delta R(t)$.[1]

Now, the relation between the driving force of spreading, derived from eq 6, and the energy dissipation is provided by the standard mechanical description of dissipative systems dynamics.[24] Because $F\{R(t)\}$ is not explicitly dependent on time, the corresponding dynamic equation will contain only two terms,

$$\frac{\partial T\{R(t); \dot{R}(t)\}}{\partial\dot{R}(t)} = \frac{\partial F\{R(t)\}}{\partial R(t)} \tag{8}$$

where $T\{R(t); \dot{R}(t)\}$ denotes the dissipation function, which

(25) Greenspan, H. P. *J. Fluid Mech.* **1978**, *84*, 125.
(26) Hocking, L. M. *J. Fluid Mech.* **1976**, *76*, 801; **1977**, *79*, 209.
(27) Shikhmurzaev, Y. D. *Phys. Fluids* **1997**, *9*, 266.
(28) Marmur, A. *J. Colloid Interface Sci.* **1997**, *186*, 462.

describes the total dissipation in a circular liquid droplet with base radius $R(t)$ and a contact line moving with velocity $\dot{R}(t)$, and the term on right-hand side determines the driving force of spreading, the derivative of the liquid/solid potential energy with respect to the base radius. Actually, eq 8 is almost verbatim the description proposed by de Gennes.[1]

Substituting eq 7 into eq 6 and performing the integration under the constraint of total volume conservation, one obtains for the driving force on the right-hand side of eq 8 the following conventional expression

$$\frac{\partial F\{R(t)\}}{\partial R(t)} = -2\pi R(t)\gamma[\cos\theta_{eq} - \cos\theta(t)] \qquad (9)$$

As a matter of fact, eq 9 ensures that the right-hand side of eq 8 vanishes (and, consequently, the spreading stops) when the droplet's base radius and the contact angle reach their equilibrium values, as prescribed by Young's equation and eq 3.

Now, following de Gennes,[1] the dissipation function can be represented as a sum of three different components,

$$T\{R(t); \dot{R}(t)\} = T\sum\nolimits_l + T\sum\nolimits_w + T\sum\nolimits_f \qquad (10)$$

where the first term describes the dissipation occurring in the immediate vicinity of the contact line, the second one describes the losses due to viscous flow in the core of the droplet, and the third one stems from the dissipative processes taking place in the precursor film. In the complete wetting case, as shown by de Gennes,[1] the third term is of crucial importance: the entire spreading power S is dissipated into the film. In the partial wetting case, however, the appearance of the precursor film is not generic. We therefore restrict our consideration to the partial wetting regime without a precursor and do not consider such dissipations here. We also hasten to remark that eq 10 implicitly presumes that the substrate is rigid and cannot be deformed by the droplet, as may occur with such soft "solids" as human skin, rubber, or elastomers. In this latter situation, one should take into account an additional dissipation channel which will result in interesting intermediate-time behavior (for example, see Shanahan and de Gennes[29] and Shanahan and Carre[30]). We will not consider such a possibility here.

Let us discuss in more detail the forms of the two remaining terms, namely, $T\sum_l$ and $T\sum_w$. Dissipation in the vicinity of the contact line results from various physicochemical processes which lead to the attachment of liquid molecules to the solid. Such a dissipation channel was considered first by Blake[18] and Cherry and Holmes[20] and subsequently scrutinized by several authors (for example, see Dodge[21] and Ruckenstein and Dunn[22] and references therein). According to Blake and Blake and Haynes,[18] the microscopic process associated with the dynamics of the contact line is the hopping motion of the fluid molecules at the edge of the droplet between adsorption sites distributed on the solid surface; the motion of the molecules at the contact line is not symmetric and they are displaced away from the droplet by molecules from the advancing liquid edge. At low velocities, the leading contribution to $T\sum_l$ is

$$T\sum\nolimits_l = 2\pi R(t)\frac{\zeta_0[\dot{R}(t)]^2}{2} \qquad (11)$$

where ζ_0 is the friction coefficient, which is determined as[18]

$$\zeta_0 = \frac{nkT}{K_w^0\lambda} \qquad (12)$$

In eq 12, T denotes the temperature, k the Boltzmann constant, n the concentration of adsorption sites, and K_w^0 and λ the typical jump frequency and length of molecular displacements, respectively. We note also that eq 11 is a simple linearized form of a more general result derived by Blake and Haynes,[18] which strictly applies for only small capillary numbers, $Ca = \eta\dot{R}(t)/\gamma$ and $Ca \ll 1$.

Next, the displacement of the contact line is followed (or preceded) by the redistribution of the fluid particles in the core of the liquid droplet, which generates a complex flow pattern. This flow pattern has been analyzed in details both experimentally and theoretically (see Dussan,[5] Dussan and Davis,[31] Bretherton,[32] and Huh and Scriven[33] and references therein). Experiments have evidenced a very characteristic rolling motion, reminiscent of a caterpillar track; i.e., the liquid velocity at the free surface, which is directed towards the advancing contact line, is larger than that inside the bulk, and liquid particles that are initially at the free surface ultimately move to the solid substrate. This rolling motion also gives rise to viscous dissipation.

To calculate the contribution of such flows to the total dissipation function, we make use of the picture introduced by Seaver and Berg[15] in their derivation of the Voinov–Hofmann–Tanner law, $R(t) \sim t^{1/10}$. The results of this oversimplified approach differ from the rigorous analysis of Cox[13] only by insignificant numerical factors. Now, Seaver and Berg assumed that the fluid dynamics of the spreading spherical cap can be approximated by that of a spreading cylindrical disk of radius $R(t)$, height h^*, and volume equal to the volume V of the droplet; see Figure 2. The height of the disk h^* is not an independent parameter but is fixed by the volume V and the radius $R(t)$,

$$h^* = \frac{R(t)}{3\phi[\theta(t)]} \qquad (13)$$

Under the assumption that the radial component V_ρ of the fluid velocity is much greater than the ξ-component, the continuity and ρ-momentum equations for the spreading cylindrical disk reduce to

$$\frac{\partial(\rho V_\rho)}{\partial\rho} = 0 \qquad (14)$$

$$\eta\left[\frac{\partial}{\partial\rho}\left(\frac{1}{\rho}\frac{\partial(\rho V_\rho)}{\partial\rho}\right) + \frac{\partial^2 V_\rho}{\partial\xi^2}\right] = 0 \qquad (15)$$

where η denotes the liquid viscosity.

Solving eqs 14 and 15 subject to the no-slip boundary condition at $\xi = 0$, Seaver and Berg found that, within the geometrical approximations involved and exclusive of the ξ-component of the flow velocity, the radial flow in the

(29) Shanahan, M. E. R.; de Gennes, P. G. *Adhesion* 11; Allen, K. W., Ed.; Elsevier Applied Science: London, 1987; p 71.
(30) Shanahan, M. E. R.; Carre, A. *Langmuir* **1995**, *11*, 1396.
(31) Dussan, E. B., V.; Davis, S. *J. Fluid. Mech.* **1974**, *65*, 71.
(32) Bretherton, F. P. *J. Fluid. Mech.* **1961**, *10*, 166.
(33) Huh, C.; Scriven, L. E. *J. Colloid Interface Sci.* **1971**, *35*, 85.

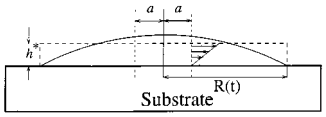

Figure 2. Seaver−Berg approximation of the flow pattern in a sessile droplet spreading on a solid substrate.

spreading droplet can be viewed as quasisteady laminar Couette flow

$$V_\rho(\rho,\xi) = A\frac{\xi}{\rho} \tag{16}$$

where A is a constant. To calculate this constant, Seaver and Berg supposed that the radial shear stress at $\xi = h^*$ was balanced by the effective radial surface tension, which yields eventually the desired Voinov−Hofmann−Tanner law for the spreading droplet. To define the dissipation in the core of the droplet due to viscous flows, we have to consider a different boundary condition at the edge of the disk. Namely, we impose the condition that the upper part of the edge moves with a prescribed velocity $\dot{R}(t)$, i.e., $V_\rho[\rho = R(t), \xi = h^*] = \dot{R}(t)$, which gives for the ρ-component of the velocity the following result:

$$V_\rho(\rho,\xi) = \frac{R(t)}{h^*\,\rho}\,\dot{R}(t) \tag{17}$$

Now, the dissipation in the core of the droplet due only to radial flows is defined by

$$T\sum\nolimits_w = \eta\int_V \mathrm{d}V\left(\frac{\partial V_\rho}{\partial\xi}\right)^2 \tag{18}$$

Substituting eq 17 into eq 18 and integrating over the droplet's volume, we find

$$T\sum\nolimits_w = 6\pi R(t)\eta\phi[\theta(t)][\dot{R}(t)]^2\ln[R(t)/a] \tag{19}$$

where the parameter a denotes the lower cutoff value of ρ. Without this cutoff, the core viscous dissipation will diverge, because the velocity at the symmery axis of the droplet has a singularity. This singularity is quite artificial, however. Clearly, instead of the singular behavior predicted by eq 17, one may expect that the radial velocity is zero at the symmetry axis and remains small within some cylindrical region of radius a centered at this axis. This is precisely the meaning of the parameter a: it is the radius of the core region, which is stagnant with respect to the radial dilation. Here, we do not attempt to determine a analytically, which would require the solution of complete momentum and continuity equations, and will use it only as an adjustable parameter, whose value will be extracted from the fit of the experimental data. We note finally that as with eq 11, eq 19 determines only the leading contribution to the dissipation in the core of the droplet, appropriate at low capillary numbers Ca.

Combining eqs 9−11 and 19, we find from the balance of forces given by eq 8 the desired dynamic equation, which describes the time evolution of the base radius or of the time-dependent contact angle in the limit of low contact line velocities:

$$\dot{R}(t) = \frac{\gamma\,[\cos\theta_{eq} - \cos\theta(t)]}{\{\zeta_0 + 6\,\eta\,\phi[\theta(t)]\,\ln[R(t)/a]\}} \tag{20}$$

or, equivalently,

$$\mathrm{Ca} = \frac{[\cos\theta_{eq} - \cos\theta(t)]}{\{\delta + 2\,\phi[\theta(t)]\,\ln(3V\phi[\theta(t)]/\pi a^3)\}} \tag{21}$$

where the parameter δ, which will be repeatedly used in what follows, is the ratio of the friction coefficient for motion of the contact line on the solid substrate and of the bulk viscosity, $\delta = \zeta_0/\eta$.

III. Comparison of Analytical Results and Experimental Data

It has been demonstrated by Ruijter et al.[34] that the results of each of the molecular kinetic and the hydrodynamic models alone can rather accurately fit experimental data. Because the equations evaluated here combine the results of both models, we may expect that they would fit experimental data at least equally as well as any of the above-mentioned approaches or any other combined approach.[23] Here, however, one may claim that the fitting parameters should be actually related to the physical characteristics of both the dissipation due to viscous flow in the core region of the droplet and to the dissipation near the contact line, because our approach is based on well-justified physical grounds.

One of the systems studied earlier[34] was a droplet of di-*n*-butylphthalate (DBP) on poly(ethyleneterephthalate) (PET) substrate.[35] At room temperature, DBP partially wets PET substrates with a very low equilibrium contact angle. The viscosity and surface tension of DBP were 19.6 mPa s and 34.3 mN/m, respectively. Here we use this set of experimental data as a tentative test of the validity of the arguments presented above. A more detailed analysis of several experimental data sets will be published elsewhere.

We fitted the current experimental data by solving eq 21, which is a first-order differential equation in R and θ, using a fourth-order Runge−Kutta algorithm.[36] Equations 3 and 4 were used to calculate the instantaneous value of the base radius from the dynamic contact angle (see Figure 3). The fitted parameters were θ_{eq}, δ, and a. The errors between the fits and the experimental data were calculated as follows:

$$E = \frac{1}{N}\sum_{i=1}^{N}|R_i^{\mathrm{c}} - R_i^{\mathrm{m}}|\frac{100}{R_0} \tag{22}$$

where N is the number of experimental data and R_i^{c} and R_i^{m} are the calculated and measured base radius at time $t(i)$, respectively. R_0 denotes the initial measured base radius. The function E can be seen as the percentage of the average error per measured datum point. The result of the fitting is shown in Figure 3 and in Table 1. The values of θ_{eq}, δ, and a for this excellent fit are respectively 0.1 degree, 130, and 1.4 μm. The average error per measurement is less than 1%.

Let us first consider the value of the cutoff, a. It is much smaller than the dimensions of the droplet (mm), so that eq 17 holds for most of the droplet. On the other hand, a is much larger than the molecular length (nm), which is consistent with the continuum description. In conclusion, the calculated value of a supports the validity of the theory

(34) de Ruijter, M. J.; De Coninck, J.; Blake, T. D.; Clarke, A.; Rankin, A. *Langmuir* **1997**, *13*, 7293.

(35) For material specifications and experimental conditions, see: Ruijter et al.[34]

(36) Press, W. H.; Teulkolsky, S. A.; Vetterling, W. T.; Flannery, B. P. *Numerical Recipes*, 2nd ed.; Cambridge University Press: New York, 1992.

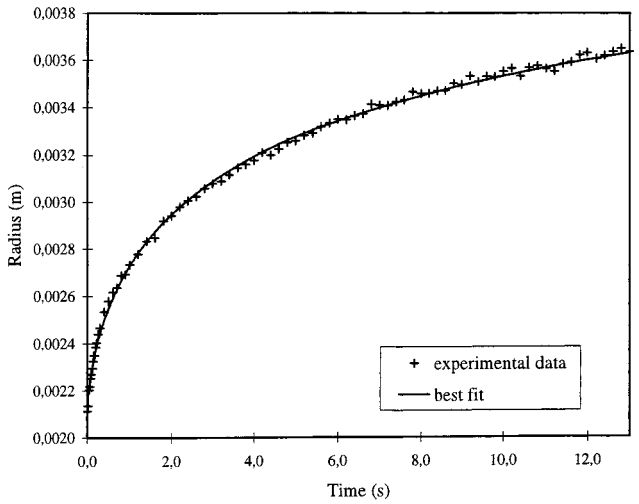

Figure 3. Contact angle relaxation of a DBP droplet on a PET substrate at room temperature. The solid line is the best fit, calculated with eq 20. The values of the fitting parameters are given in Table 1.

Table 1. Comparison of the Fitting Parameters Using Different Models[a]

model	a (m)	δ	E (%)
combined	$(1.4 \pm 0.2) \times 10^{-6}$	130 ± 15	0.6
hydrodynamic	$(4.4 \pm 0.4) \times 10^{-8}$	0	1.2
molecular−kinetic		330 ± 40	0.7

[a] The errors on a and δ are calculated with the bootstrap method,[34,36] assuming a standard deviation of 1° on the individual contact angle measurements.

together with the assumptions underlying the derivation of eq 20. The large value of δ indicates that the friction due to the bulk flow is much smaller than the friction in the vicinity of the contact line. From δ, the friction coefficient near the contact line ζ_0 is 2.6 Pa s. Thus, the assumption of the hydrodynamic approach, namely, that the dissipation near the contact line may be omitted, is not appropriate for the liquid/solid system under consideration. This was also pointed out earlier.[34]

Next, let us consider how the experimental data can be fitted by the results of the hydrodynamic approach only. If δ in eq 21 is forced to be 0, the equation becomes purely hydrodynamic. Using this condition and the same set of experimental data (see Figure 4), we find that a is approximately 0.044 μm (Table 1). To compensate for the dissipation near the contact line, a has to be smaller than the value calculated before. The fit is not as good as before, but the modified equation still models the data very well (error is only about 1.2%).

Let us consider the fit of the experimental data using the result of the molecular kinetic model only. We note that eq 20 will reduce to the result of the linear capillary number version of the Blake and Haynes molecular kinetic theory if we discard the second term in the denominator by setting, for instance, $\eta = 0$. The best fit under this condition is also shown in Figure 4. This time, the fit is better except at very early times. The δ is now 330, indicating that by using only the molecular kinetic theory, we overestimate the friction near the contact line.

In conclusion, if only the dissipation in the bulk (hydrodynamic model) or only the dissipation near the contact line (molecular kinetic model) is considered, the experimental data can still be fitted quite well. However, the fitting parameters are adjusted to compensate for the omitted dissipation channels and therefore lose some of their physical meaning.

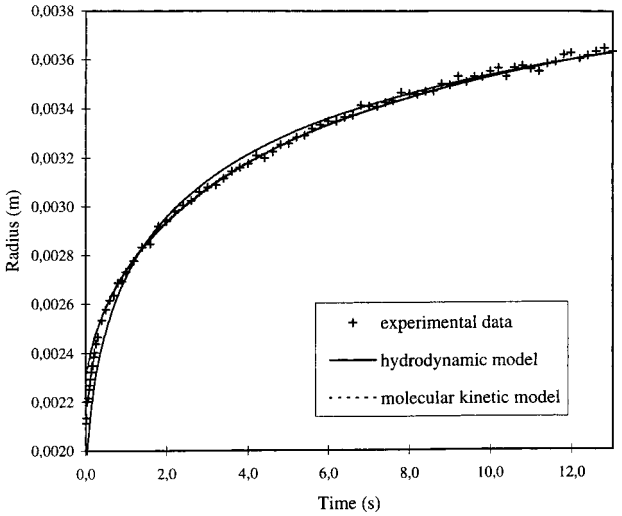

Figure 4. Contact angle relaxation of a DBP droplet on PET substrate at room temperature. The solid line represents the best fit with the hydrodynamic model, eq 20 with $\zeta_0 = 0$. The dashed line is the best fit with the molecular kinetic model, eq 20 with $\eta = 0$. The best values for both fits are given in Table 1.

IV. Asymptotic Solutions of the Dynamical Equations

Early-Time Dynamics. Let us consider first the solution of eq 20 in the limit of short times, supposing, for simplicity, that $\theta_0 \approx \pi/2$. We find then from eq 20 that for sufficiently small deviations from the initial values of the base radius and the contact angle such that

$$R(t) - R_0 \ll \frac{R_0}{\ln(3V/2\pi a^3)} \tag{23}$$

$$\theta_0 - \theta(t) \ll \frac{2}{\ln(3V/2\pi a^3)} \tag{24}$$

these properties obey

$$R(t) = R_0 + \frac{\gamma \cos \theta_{eq}}{\zeta_0 + \eta} t \tag{25}$$

and

$$\theta(t) = \theta_0 - \left(\frac{16\pi}{3V}\right)^{1/3} \frac{\gamma \cos \theta_{eq}}{\zeta_0 + \eta} t \tag{26}$$

Substituting eqs 25 and 26 into eqs 23 and 24, we thus infer that this early-time linear dependence on time persists until $t < t_1$, where

$$t_1 \approx \frac{(\zeta_0 + \eta) R_0}{\gamma \cos \theta_{eq} \ln(3V/2\pi a^3)} \tag{27}$$

Intermediate-Time Dynamics. At intermediate times, i.e., such that $t \gg t_1$ but still much less than the time at which $R(t)$ reaches its equilibrium value, it is not possible, of course, to obtain simple scaling laws for $R(t)$ of the form $R(t) \sim t^{\alpha}$. This becomes possible only when $\theta_{eq} \ll \pi/2$ and the contact angle $\theta(t)$ gets sufficiently small such that the expansion of the trigonometric functions in their Taylor series up to the second power of $\theta(t)$ is justified. In this

limit, eq 21 simplifies considerably:

$$\mathrm{Ca}\{2\delta\theta(t) + {}^{16}/_{3}\ln[4V/\pi a^3\theta(t)]\} = \theta(t)^3 - \theta(t)\theta_{eq}^2 \quad (28)$$

In the limit $\delta \approx 0$, i.e., the limit when friction in the vicinity of the contact line is negligibly small, eq 28 resembles, apart from the logarithmic factors, the results obtained earlier by de Gennes[37] and Seaver and Berg.[15] Equation 28 shows that in particular situations two different types of scaling behavior can be observed at this intermediate-time stage. For $\theta(t)$, which is small enough to ensure expansion of the trigonometric functions into the Taylor series, but still larger than some θ_c, which are approximately defined as

$$\theta_c \approx \frac{8\ln(4V/\pi a^3)}{3\delta} \quad (29)$$

the first term in the brackets on the left-hand side of eq 28 is the dominant one. Consequently, one should observe at this stage

$$R(t) \sim \left(\frac{2V}{\pi}\right)^{2/7}\left(\frac{14\gamma t}{\zeta_0}\right)^{1/7} \quad (30)$$

or, for the dynamic contact angle,

$$\theta(t) \sim 2\left(\frac{2V}{\pi}\right)^{1/7}\left(\frac{14\gamma t}{\zeta_0}\right)^{-3/7} \quad (31)$$

i.e., exactly the behavior predicted by the molecular kinetic approach.[18,21] Using eqs 29−31, we can thus define the characteristic time until the scaling behavior $R(t) \sim t^{1/7}$ is valid. Substituting eq 31 into eq 29, we find that eqs 30 and 31 can exist for times less than a certain t_2, which equals

$$t_2 \approx \frac{\zeta_0 V^{1/3}}{2\gamma}\left(\frac{\delta}{\ln(V/a^3)}\right)^{7/3} \quad (32)$$

This time can be sufficiently large, if the droplet's volume is large or δ is large. In this case, the regime described by eqs 30 and 31 may persist over a wide time interval.

At times greater than t_2, but such that $R(t)$ is still less than its equilibrium value, we will observe the crossover to the Voinov−Hofmann−Tanner-type behavior

$$R(t) \sim \left(\frac{2V}{\pi}\right)^{3/10}\left(\frac{15\gamma t}{\eta\ln(3V/\pi a^3)}\right)^{1/10} \quad (33)$$

or, for the dynamical contact angle,

$$\theta(t) \sim 2\left(\frac{2V}{\pi}\right)^{1/10}\left(\frac{15\gamma t}{\eta\ln(3V/\pi a^3)}\right)^{-3/10} \quad (34)$$

We note here that the crossover time t_2 appears to be a fundamental parameter, which distinguishes which of the dissipation channels will dominate on the scale of experiments. Apparently, those experiments which show the departure from the $R(t) \sim t^{1/10}$ behavior are performed with liquid/solid systems with characteristic time t_2 sufficiently large compared to the time scale of observation. On the other hand, experiments which reveal such a law are done with systems with low values of t_2. In particular, the experimental data of Dodge,[21] which favor the molecular kinetic prediction, i.e., $R(t) \sim t^{1/7}$, were obtained for droplets composed of PDMS−OH molecules. These polymers form strong chemical bonds with solid substrates and consequently one can expect that for such systems ζ_0 and t_2 are large, so that the behavior predicted by eq 31 persists over an extended time interval. We note also that the trend observed by Sawicki[17] is in complete qualitative agreement with our results; namely, t_2, eq 32, depends strongly on the liquid's viscosity, $t_2 \sim \eta^{-7/3}$, and thus can be very large for low-viscosity liquids.

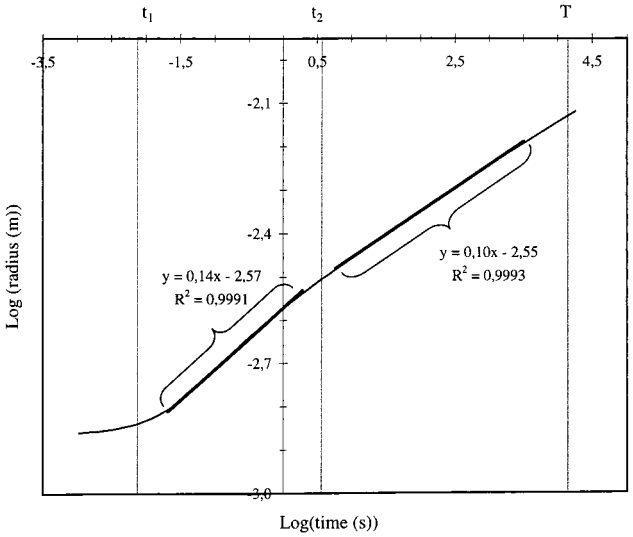

Figure 5. Equation 20 with $\theta_{eq} = 0.1$, $a = 1.4\,\mu$m, and $\delta = 130$. The values of t_1, t_2 and T are calculated with, respectively, eqs 27, 32, and 37. Two distinguished parts of the curve are fit by linear regression as indicated.

Long-Time Relaxation to Equilibrium. Let us consider finally the long-time behavior of the droplet when it approaches the equilibrium shape. Representing the base radius as $R(t) = R_{eq} - \delta R(t)$ and $\theta(t)$ as $\theta(t) = \theta_{eq} + \delta\theta(t)$, where $\delta R(t)$ and $\delta\theta(t)$ denote small derivation[38] from the equilibrium values, substituting these expressions into eq 28 and accounting for only linear terms, we have

$$\frac{\delta\dot{R}(t)}{\delta R(t)} \approx -\frac{3\gamma\theta_{eq}^2}{\eta R_{eq}[\delta + 8\ln(3V/\pi a^3\theta_{eq})/3\theta_{eq}]} \quad (35)$$

which yields

$$\delta R(t) \approx \exp\left(-\frac{t}{T}\right) \quad (36)$$

with

$$T = \frac{\eta R_{eq}[\delta + 8\ln(3V/\pi a^3\theta_{eq})/3\theta_{eq}]}{3\gamma\theta_{eq}^2} \quad (37)$$

We note that such an exponential form, with T treated as an adjustable parameter, has been successfully used to fit experimental data by Newman.[39] Our work thus provides an explicit interpretation of the characteristic time T in terms of the liquid/solid system parameters.

Let us now reconsider the experimental data presented above. Using the best values for θ_{eq}, a, and δ, we can extrapolate the spreading behavior of our liquid/solid system at different time scales. In Figure 5, we show the whole time range, from milliseconds up to hours of

(37) de Gennes, P. G. *Z. Kolloid Polym. Sci.* **1986**, *264*, 463.

(38) We note that $\delta R(t)$ and $\delta\theta(t)$ are not independent but related to each other because of the volume conservation condition.

(39) Newman, S. *J. Colloid Interface Sci.* **1968**, *26*, 209.

spreading, in a log−log plot but within the constraints of $Ca < 1$ and $\theta < 90$. The calculated values for t_1, t_2, and T are 8.0×10^{-3}, 4.5, and 1.5×10^4 s, respectively. In Figure 5, it is shown that the time frame between t_1 and t_2 can best be fitted by a straight line with slope 0.14, very close to the expected $^1/_7$. Above t_2, the curve is best-fitted by a straight line with slope 0.10, which is exactly the predicted value. At times around T, the curve starts to deviate from this linear fit. This is an explanation for the different power laws which have been reported in the literature. When concentrating on systems "far" from equilibrium, as is mostly the case in forced wetting experiments, the molecular kinetic theory should fit the data very well. On the other hand, when systems are studied close to equilibrium, we are likely to find the power law predicted by the hydrodynamic models or, at very long times, to find an exponential behavior.

Our experiments fall within the 10^{-2}−10 s time frame, around the value of t_2. This is exactly the reason why we could fit our data almost equally well with the hydrodynamic model as with the molecular kinetic one.

V. Concluding Remarks

Using a combined dissipation channel approach, we obtained a macroscopic analytical description of droplet spreading on a solid surface in situations appropriate for partial wetting. We have shown that in the general case a succession of several different regimes can be observed. Namely, (1) a fast early-time stage characterized by a linear time-dependence of the base radius; (2) a kinetic stage at which the dominant contribution to dissipation comes from attachment of fluid molecules to a solid and the time evolution of the base radius is compatible with the predictions of the molecular kinetic approaches;[18] (3) a kinetic stage at which the hydrodynamic dissipation dominates; and lastly, (4) an exponential relaxation to the equilibrium state. Analyzing experimental data along these lines allows us to obtain meaningful values for the molecular friction and the necessary cut-off distance.

Acknowledgment. The authors gratefully acknowledge fruitful and encouraging discussions with Prof. A-M. Cazabat and Dr. T. Blake. M.d.R. thanks Kodak European Research Laboratories for their hospitality during his visit and Dr. A. Clarke for his kind assistance in experimental measurements. This research was supported by the FNRS, the European Community through the Grant CHRX-CT94-0448, the COST Project D5/0003/95, PROCOPE-programme, and by the Ministère de la Région Wallone.

LA971301Y